International Journal of Fatigue 166 (2023) 107239

Contents lists available at ScienceDirect

International Journal of Fatigue

journal homepage: www.elsevier.com/locate/ijfatigue

Approaches to fatigue lifing in a high strength polycrystalline nickel alloy

M.T. Whittaker [a,*], N.C. Barnard [a], B.J. Cockings [a], E. Duffy [a], S.J. Williams [b], M.C. Hardy [a]

[a] Institute of Structural Materials, College of Engineering, Swansea University, Swansea SA1 8EN, United Kingdom
[b] Rolls-Royce PLC, PO Box 31, Derby DE24 8BJ, United Kingdom

ARTICLE INFO

Keywords:
Fatigue
Melt anomaly
Notches
Walker strain

ABSTRACT

The development of high strength alloys with complex chemistries has led to modern nickel disc alloys being produced through a powder metallurgy process which often produces melt anomalies within the material microstructure. The current research investigates the effect of these melt anomalies on overall lifing approaches for the alloy RR1000, utilised here in its fine grained form. A Walker strain approach is applied to investigate the effect of temperature and R ratio on lifing parameters, and a temperature dependent version of the equation is suggested and used to produce predictions of notched specimen fatigue behaviour. It is found that hard particle inclusions dominate fatigue failures at long fatigue lives whereas failure occurred at the peened surface for shorter fatigue lives. However, lifing approaches were able to provide good fits across the entire data set irrespective of this behaviour change.

1. Introduction

The gas turbine sector has produced remarkable growth since its inception in the 1940s with the constant requirement for increased reliability, economy and performance coupled with cost reduction providing an extremely challenging environment. Whilst this has been achieved through a wide range of innovative engineering applications, significant credit must be given to the development of a catalogue of materials which have been utilised for challenging applications in extremely arduous environments. Despite the advances already made, future requirements are equally as challenging due to the fuel, CO_2, NO_x and noise reductions proposed by the ACARE 2020 [1] and more latterly Flightpath 2050 targets [2].

Fortunately the field of materials development continues to provide appropriate solutions through new alloy development, innovative processing/application and step changes in technology towards composite materials. In the area of disc manufacture however, nickel alloys continue to dominate due to their combination of high strength, damage tolerance, high temperature capability and good corrosion resistance. In order to improve efficiency, weight savings and higher operating temperatures can provide significant cost savings due to the large nature of the components, and as such, alloy development in the field is extremely active.

It is difficult to increase strength in these alloys without property reductions in other areas [3], and consequently sensitivity to potential defects in the microstructure is an area that has become heightened in more modern alloys. In particular, the potential for melt anomalies in the microstructure is of significant interest in deriving appropriate fatigue life predictions. Indeed, it is critical for modern alloys which contain complex chemistries that alloys are manufactured using a powder metallurgy route in order to minimise segregation [4], which is common in material produced by conventional cast and wrought techniques. However, whilst reduced by careful processing methods, anomalies still occur and the impact on mechanical behaviour requires analysis.

In particular, melt anomalies tend to occur as ceramic inclusions brought about by the use of the powder metallurgy process and can occur in the melt, during powder atomization or during any of the various handling processes through consolidation [5]. The effect of melt anomalies and non-metallic inclusions on the mechanical performance of various nickel based superalloys is well documented, with powder metallurgy processed materials known to be particularly sensitive to these defects under fatigue loading [6]. In particular the differences in the coefficient of thermal expansion between the metallic alloy and potentially ceramic inclusion may lead to debonding of the inclusion from the matrix, or even cracking of the inclusion. Jablonski found that ceramic inclusions did not substantially reduce the fatigue life at room temperature, but were far more detrimental at 500 °C. [7]. The author attributed this to the fact that the inclusion debonded at room temperature, but cracked at elevated temperature, and that this cracked

* Corresponding author.
E-mail address: m.t.whittaker@swansea.ac.uk (M.T. Whittaker).

https://doi.org/10.1016/j.ijfatigue.2022.107239
Received 22 December 2021; Received in revised form 25 July 2022; Accepted 2 September 2022
Available online 7 September 2022

inclusion provided a larger and sharper initial starter crack. Hyzak and Bernstein [8] similarly found that at high strain ranges crack initiation from these defects occurred early in the test and hence fatigue life was determined more by a combination of defect location and size, along with crack propagation behaviour. Jha et al [9] considered the effect of the position of melt anomalies with regards to surface cutting or sub-surface particles and consistent with the work by Gabb et al [5] recognised surface cutting inclusions to be particularly detrimental. Shamblin and Chang [10] provided a more detailed analysis of the types of inclusions in René 95, identifying two major types which contributed to significant fatigue life degradation, namely prior particle boundary decoration type inclusions, and also discrete ceramic type inclusions. Previous work [11] has also considered in the effects the nickel based superalloy Rene' 88, in which a controlled distribution of ceramic seeds was added to the material to simulate in service melt anomalies. The work considered the effects of two sizes of deliberately seeded ceramic particles. At low temperatures very little effect was found from the ceramic seeds with the majority of fatigue failures initiating from grain facets. Peening was found to have a negligible influence on the fatigue life of specimens (although the initiation sites were generally suppressed to sites below the surface). However, for higher temperatures the situation is significantly different with inclusion based failures now dominating, and life being strongly correlated to initiation size. Further complex interactions were observed between seed size and peening effects, which require consideration in the current work.

2. Experimental methods

The material considered for this study was the powder metallurgy produced nickel-based superalloy RR1000, the chemical composition of which can be seen in Table 1.

The alloy was supplied by Rolls-Royce in the form of solid round bar specimens, Fig. 1, with a 9 mm diameter, with the aim of maximising the material volume to be tested. Specimens were extracted from a rotor disc forging, which had been produced by conventional power metallurgy method, low strain rate isothermal forging and subsequent heat treatment to generate the desired microstructure. In particular, fine grained RR1000 was tested for this research program, with an average grain size of 5–10 μm as per ASTM E112. As-received specimens were shot peened to Rolls-Royce in-house specifications, in order to produce a compressive residual stress layer at the specimen surface.

The specimens were tested under strain control to BS7270 [12] on a range of servo hydraulic and electric screw machines using controlling MTS high temperature extensometers with gauge lengths of 25 mm. The experiments were completed using a trapezoidal waveform with a ramp rate of 0.5 %/*sec* and 1 s hold at peak and minimum strains. Testing was completed over a range of temperatures from 20 to 750 °C with R ratios of −1, 0, 0.3 and 0.5. Stress–strain loops were recorded by data logging systems which also allowed the recording of peak and minimum stresses so that a graph of stress evolution as a function of cycles could be derived. Upon reaching a stabilised condition (approximately 20,000 cycles) tests were switched to a servo hydraulic test frame and were continued to failure under an accelerated load control phase, using a sine waveform at a frequency greater than 4 Hz. Experiments conducted at the start of the programme indicated that this method of accelerated testing has negligible effects on fatigue life, similar to previous work in the field [13].

3. Results

As part of a large-scale testing programme for RR1000, fine grained RR1000 samples were tested to failure or a run out condition of 10^7 cycles, under a variety of R ratios. The data is represented in Fig. 2 as Walker strain [14] against cycles to failure. For the current work, the Walker strain equation was utilised in order to provide a lifing correlation. In the past the Walker strain equation has been widely used for R ratio correction [15,16], but an aim of the current work is to investigate its ability to correct for temperature alongside R ratio. The Walker strain equation can be utilised in the form

$$\Delta\varepsilon_w = \frac{\sigma_{\max}}{E}\left(\frac{\Delta\varepsilon E}{\sigma_{\max}}\right)^m$$

where; $\Delta\varepsilon_w$ = Walker strain

σ_{max} = maximum stabilised stress
E = Modulus
$\Delta\varepsilon$ = strain range
m = Walker exponent

In order to develop a lifing approach for the material, a range of correlative methods can be applied to the data to attempt to remove dependence on temperature and R ratio and provide a simple method of life prediction. These methods may be either stress based (e.g. Basquin [17]) or strain based (etc Manson-Coffin [18,19], Morrow [20]). For the current material, since applications are likely to be dominated by strain controlled environments due to restriction by surrounding material or localised non-linear features, a strain based methodology would be preferable. Previous experience has shown the Walker strain method to be an appropriate methodology when mean stresses play a significant role [21] although the Morrow approach offers similar benefits. Work by other researchers has also shown successful implementation of the Smith-Watson-Topper approach [6].

The strain control data produced for different R ratios is first correlated by the Walker strain equation using an appropriate m value. This was determined to be 0.72 over the entire temperature range. Curve fitting the correlated data gives the expression.

$$\Delta\varepsilon_w = aN^b$$

where for the complete set of data, a = 0.0141 and b = −0.067. Based on these parameters, predictions can be made for the fatigue lives of specimens using only this simplistic Walker equation. More specifically, the predictions therefore examine the capability of the Walker equation to accommodate both R ratio and temperature variations by a single correlative technique.

Despite the clear benefits of a single relationship to govern behaviour across all temperatures, it is perhaps more appropriate to consider the equation at individual temperatures. It is found that a strong trend is observed between temperature and m value. Since this exponent controls the contribution of the range based term in the Walker equation, analysis of its behaviour can aid in determining controlling parameters. Clearly, based on the results shown in Table 2, it is apparent that tests conducted at lower temperatures show a low exponent value, and therefore the fatigue lives are dominated mainly by the peak stabilised stress achieved during the test. Since the specimens typically cyclically harden at this temperature it is clear that any variation of the peak stress significantly influences fatigue life, whereas the extent of specimen unloading is of minimal importance. With the m value increasing almost

Table 1
Chemical composition of RR1000.

	Co	Cr	Mo	Ti	Al	Ta	Hf	Zr	C	B	Ni
Weight %	18.5	15	5	3.6	3	2	0.5	0.06	0.03	0.02	Bal

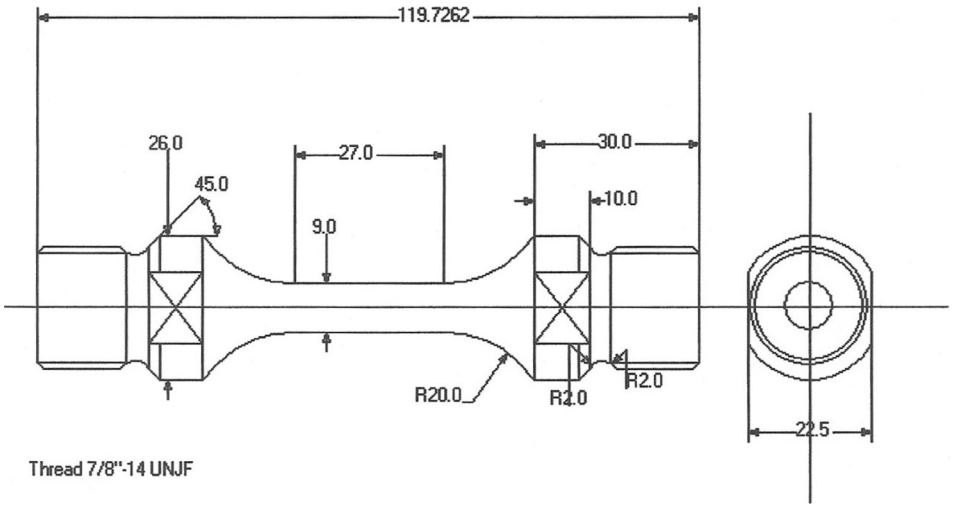

Fig. 1. Dimensions for tested specimens.

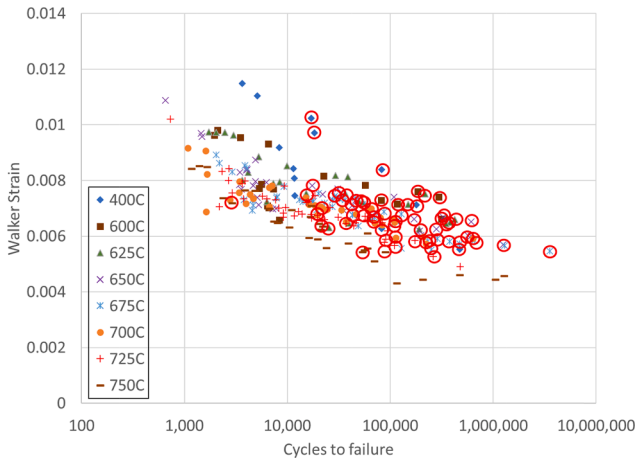

Fig. 2. Data generated within the programme represented as Walker strain vs Cycles to failure (m = 0.72). Subsurface failures are circled in red.

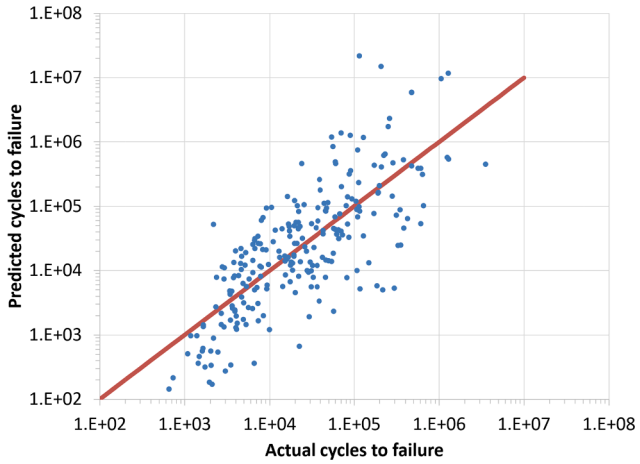

Fig. 3. Predicted lives for entire dataset using a Walker strain equation with a single exponent (0.72) for all temperatures.

Table 2
Walker strain parameters as a function of temperature.

Temperature (°C)	m	A	b
400	0.15	0.0102	−0.05
600	0.33	0.0091	−0.037
625	0.43	0.0106	−0.047
650	0.45	0.0102	−0.044
675	0.58	0.0115	−0.054
700	0.66	0.0113	−0.051
725	0.76	0.0161	−0.085
750	0.92	0.0223	−0.119

to unity at the higher temperatures, fatigue life is now influenced by both the peak stress and stress range more equally.

3.1. Failure analysis of fine grained RR1000

In examining the failure types of the RR1000 specimens, a clear demarcation between surface and subsurface failures is seen to occur at intermediate fatigue lives, shown in Fig. 2 where sub-surface crack initiations are circled in red. Macro images of subsurface and surface failures are provided in Fig. 4. Following intital examination at low magnification, further analysis of the initiating feature could be conducted through high magnification scanning electron microscopy.

Interestingly, the change in behaviour appeared to be independent of R ratio, and therefore, the initial plastic strain applied to the specimen upon the initial loading cycle. Instead when plotted on the basis of fatigue life as a function of applied strain range, specimens with higher strain ranges failed consistently from the peened surface. Apart from a transition region around an intermediate strain range, for lower values of applied strain range, tested specimens again showed a remarkable consistency in failure mechanism, failing almost solely from subsurface features which occur during processing of the alloy by a powder metallurgy process. Consistent with previous studies [22], these melt anomaly failures could be classified into four predominant anomaly types, as shown in Fig. 5. It can be seen that these non-metallic inclusions were either (a) small grouped inclusions (b) large blocky inclusion surrounded by halo of smaller inclusions (c) large faceted inclusion with surrounding smaller grouped inclusions (d) large blocky inclusion with associated local faceting. Work by Zhang et al [23] has shown similar features in the same alloy with EDS spectra confirming Al and Hf oxides. The blocky inclusions in Fig. 5 (b), (c) and (d) are typical oxide inclusions from refractory ceramics used in powder manufacture [24] whereas the small oxide particles in Fig. 5(a) are a consequence of a

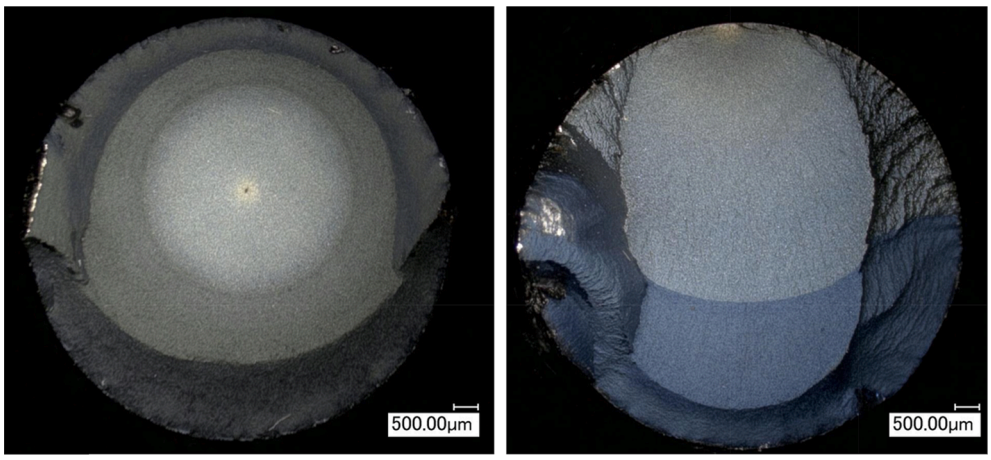

Fig. 4. a) Subsurface failure in RR1000, 675 °C, R = 0, ε_{max} = 0.8 % (b) Surface failure in RR1000, 700 °C, R = 0.33, ε_{max} = 1.1 %.

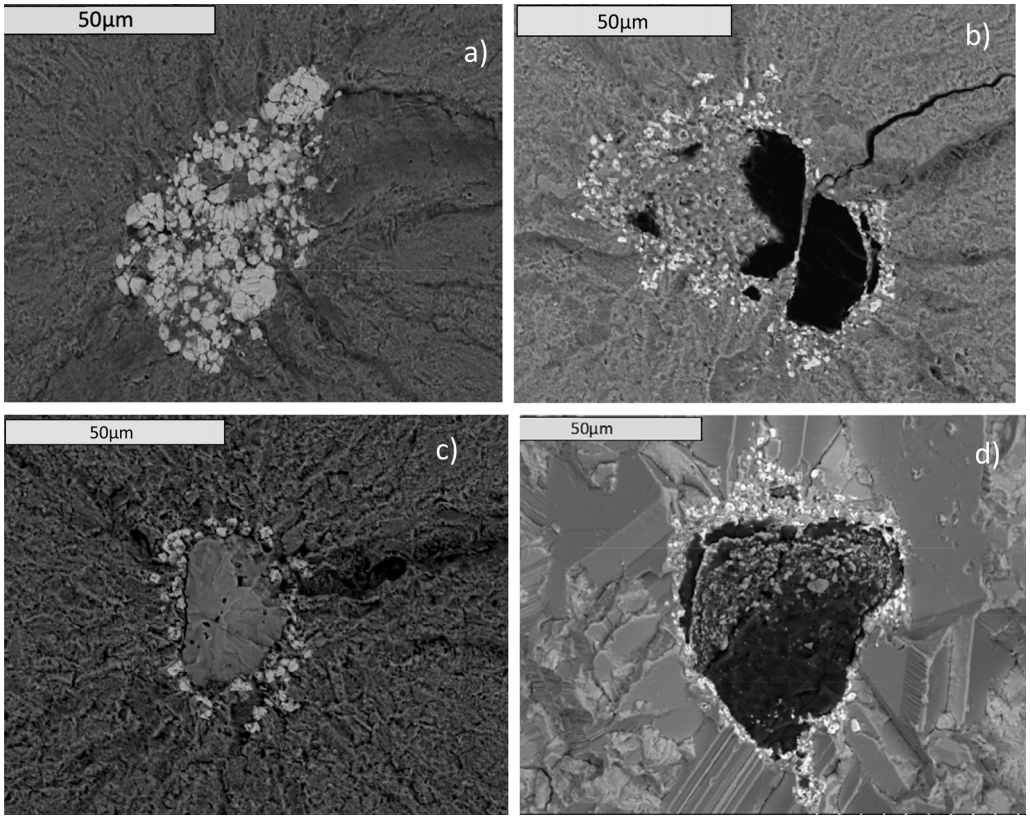

Fig. 5. Subsurface failure types in RR1000 (a) Small grouped inclusions (b) Large blocky inclusion surrounded by halo of smaller inclusions (c) Large faceted inclusion with surrounding smaller grouped inclusions (d) Large blocky inclusion with associated local faceting.

reactive element in the alloy composition. It appears that in the cases of a), c) and d) that decoupling between the inclusion and the matrix has occurred which has initiated the fatigue crack, whereas in b) the crack has initiated as a result of fracture of inclusions.

Interestingly, the type of inclusion, along with the size, shape and depth, appeared to have minimal effect on the fatigue life of specimens. Indeed, the high cycle fatigue specimens which failed from subsurface melt anomalies form a relatively continuous fatigue curve with the low cycles fatigue surface failures. A lower band of failures at 750 °C can be seen in Fig. 2, where oxidation is likely to promote early crack growth from the specimen surface [25].

4. Discussion

In attempting to generate a lifing approach for the alloy across a range of temperatures, it quickly becomes clear that data generated at 400 °C does not correlate well with the total dataset. In particular, R = −1 data stands out when attempting to generate an appropriate response using the Walker strain equation. From the previous data shown, it is apparent that a far lower exponent is required to correlate the data at this temperature, although it should be noted that data is only available for two R ratios (R = −1 and R = 0.5, with a single point for R = 0) whereas larger data sets are available at many other temperatures. Nevertheless, the exponent generally follows the trend demonstrated by the values at all other temperatures and is optimised for a value of 0.16.

Such a low value of the exponent in the Walker equation indicates that the fatigue life of specimens at this temperature is dominated by the maximum stress achieved during testing, rather than the stress range. Analysis of the data also shows that at this temperature, the deformation behaviour of the material is dominated by isotropic hardening, with clear examples shown in both R = −1 and R = 0 tests, Fig. 6(a) and (b). This is a trend which is not repeated at higher temperatures, with only sporadic examples of isotropic hardening. Depending on the maximum applied stress in the tests, the deformation behaviour tends to be a mix of kinematic hardening and isotropic softening, Fig. 6(c). Subsequently the increased value of the Walker exponent at higher temperatures is indicative of a stronger contribution from the stress range to the overall fatigue life. It is particularly interesting that the value of the Walker exponent shows a near linear relationship with increasing temperature since this provides a potential opportunity for development of the Walker equation in order to more accurately collapse both R ratio and temperature data.

The transition from surface based failures to subsurface was relatively consistent in terms of fatigue life, with very few surface failures occurring with fatigue lives above 100,000 cycles. Generally, the only exception to this was for the fatigue tests conducted at 750 °C, where a significant reduction in the fatigue life was often accompanied by a surface failure. The reduction in fatigue life under these high cycle fatigue conditions seems to indicate an increased sensitivity to surface condition rather than a deactivation of the mechanism controlling subsurface failures, since the fatigue lives are reduced from what would generally be anticipated by extrapolation of lower temperature data. With increased oxidation now becoming a significant factor at this elevated temperature, oxide nodules on the surface have been shown to be a significant factor in crack initiation.

The transition itself between surface and subsurface behaviour is a direct function of applied strain range, rather than peak strain which might be anticipated. Indeed, the transition from fully elastic to plastic deformation at the yield stress does not play a role in this change in failure mechanism, as has been observed by comparing the results of fully elastic R = −1 tests with R = 0.5 tests significantly above the yield stress, both of which can produce fatigue lives in excess of 100,000 cycles and failures from sub surface melt anomalies. The transition is actually a function of the onset of continuous plastic deformation within the material, with R = −1, R = 0 and R = 0.5 loops essentially indistinguishable in shape when considered from a nominal stress–strain coordinate, and surface based initiations only occurring when the strain range is large enough to provide continually open hysteresis loops. Presumably in order to initiate the fatigue process through the development of surface intrusions/extrusions, this repeated plastic deformation is required as dislocations overcome γ' particles either through shearing at low temperatures or thermally activated processes such as diffusion controlled dislocation climb at higher temperatures. Unsurprisingly, the fact that surface based failures tend to show a fatigue curve with a slightly poorer performance than for sub surface failures, indicates that the alloy is especially sensitive to surface damage, hence the importance of shot peening. Failures at high strains tend to be dominated by significant amounts of plasticity, and therefore are relatively insensitive to surface finish. As demonstrated, below a critical applied strain range surface failures are not initiated in preference to subsurface crack development. Therefore surface finish plays an important role only in transition region of strains at or slightly above the onset of continuous plastic deformation.

Analysis of this dataset showed that the fatigue lives of subsurface failures appear insensitive to size, shape and distribution when sub surface. The largest melt anomalies were found to be the small grouped inclusions shown in Fig. 5(a). The fatigue life of this specimen was

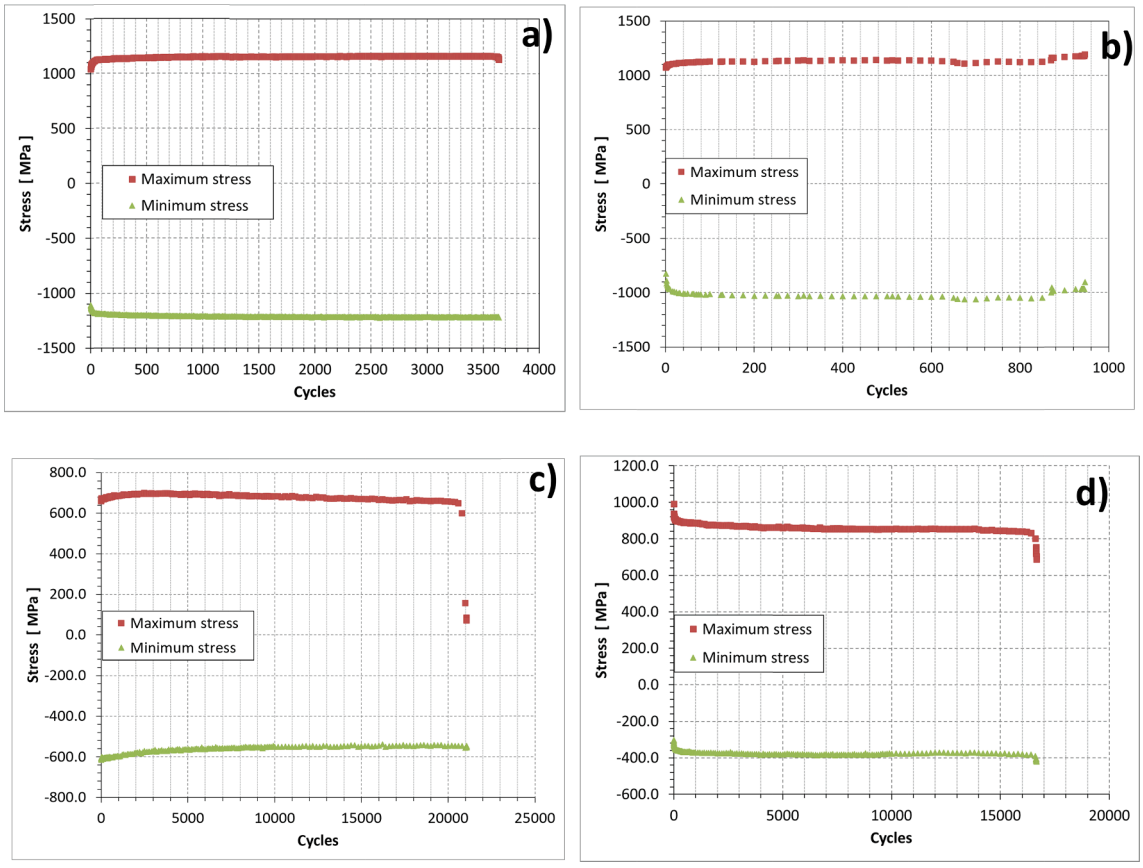

Fig. 6. (a) Isotropic hardening at 400 °C, R = −1, ε_{max} = 0.75 %, (b) Isotropic hardening at 400 °C, R = 0, ε_{max} = 1.2 %, (c) Kinematic hardening at 750 °C, R = −1, ε_{max} = 0.75 % (d) Kinematic softening at 750 °C, R = 0, ε_{max} = 0.75 %.

116,806 cycles, as opposed to the predicted life of 503779, a variation which does not fall outside of the normal scatter within the data. The data was investigated to ascertain whether a relationship could be found between fatigue life and parameters such as failure location, subsurface inclusion size, subsurface inclusion depth etc, but no trend was found of fatigue life showing a strong dependence of any of these parameters. This is encouraging in terms of component lifing since it indicates that typical melt inclusions in the current alloys do not significantly affect fatigue life and can be lifed using a similar and extended approach to surface failures at shorter fatigue lives.

Infrequently, samples failed from a surface initiation, where a melt anomaly cut the surface of the specimen. It was noted that in the current programme of fatigue tests, only 6 failed from surface cutting inclusions and therefore may not be statistically significant. It should be noted that in specimen testing this number would be expected to be significantly higher than for in-service conditions due to the increased surface/volume ratio in the tested specimens compared with large scale components. However, the possibility of such failures in-service still applies and requires consideration.

The mechanism of failure of the large faceted inclusions appeared to be shearing of this hard particle, similar to that found by Jablonski [7], evident by the same size and shape of inclusion being observed on both fracture surfaces. Presumably this is due to increased shear stress at the interface between the base material and the anomaly brought about by dislocation pile up. Fig. 5(b) shows an example of an large blocky inclusion, surrounded smaller grouped inclusions, which has fractured, with the offset between the fractured surfaces supporting the sheared particle assumption. Where the anomalies are defined as small grouped inclusions, the particles appear to suffer from matrix/inclusion decoupling which initiates the fatigue crack, Fig. 7, similar to that previously shown by Zhang and Dunne [26].

The ability of the Walker equation to provide a single correlation for the entire data set has been evaluated in this work. The Walker strain approach was developed as a mechanism of R ratio correction which the current authors have found to be more applicable than traditional approaches involving the Manson-Coffin equation. However, the Walker equation is often used to collapse both R ratio and temperature data using only the single parameter, *m*. By making this parameter more explicitly temperature dependent, the potential for more accurate fitting is provided. In the current work, the noticeable trend of increasing exponent value with temperature potentially allows for development of the Walker strain equation. For the current example the 400 °C data has not been considered since derivation of the Walker exponent is slightly more arbitrary due to having only two sets of R ratio data. Furthermore the material behaviour differs significantly to that shown at higher temperatures, and whilst a linear extrapolation would not be a particularly poor fit for the exponent at this temperature, it would be at the detriment of the high temperature values.

A simple linear fit of the exponent value for 600–750 °C produces the following relationship

$$m = \alpha T + \beta$$

where m is the Walker exponent and T is temperature and the fitting parameters $\alpha = 0.0038$ and $\beta = -1.9557$. Utilising these values in a temperature dependent Walker equation therefore yields

$$\varepsilon_W = \left(\frac{\sigma_{max}}{E}\right)\left(\frac{\Delta\varepsilon E}{\sigma_{max}}\right)^{\alpha T+\beta}$$

and a simple power law fit to a graph of cycles to failure as a function of Walker strain allows for prediction of fatigue lives across the temperature range 600–750 °C utilisng only this simple equation, Fig. 8.

In order to evaluate the effectiveness of the predictions, it is possible to utilise the Mean Squared Error (MSE) approach. Letting y_i^a be the experimental (or actual) value for the fatigue test, obtained at the ith test condition and y_i^p the predicted fatigue life based on the Walker strain approach, the MSE is given by

$$\text{MSE} = \frac{\sum_{i=1}^{n}\left(y_i^a - y_i^p\right)^2}{n}$$

where there are n fatigue tests. Squares are taken to prevent under predictions being offset by over predictions. To make it easier to compare the accuracy of the two models, the MSE can be re-scaled to be within the range zero to unity as follows

$$U = \frac{\sqrt{\frac{1}{n}\sum_{i=1}^{n}\left(y_i^a - y_i^p\right)^2}}{\sqrt{\frac{1}{n}\sum_{i=1}^{n}\left(y_i^a\right)^2} + \sqrt{\frac{1}{n}\sum_{i=1}^{n}\left(y_i^p\right)^2}}$$

From the current testing a U value of 0.84 is found from the simple Walker approach, Fig. 3. However, utilising a temperature dependent Walker approach as described above reduced this value to 0.71, indicating a significant improvement over the traditional method. Whilst it is apparent that there are many outliers to the predictions, there is no consistent pattern to these points. It is possible that overpredictions occur when melt anomalies occur at or close to the surface, consistent with the findings elsewhere [5,9] and that underpredictions occur where no significant anomaly occurs within the testpiece.

Clearly it is desirable to understand the fundamental behaviour of the material using plain, cylindrical specimens in order to develop

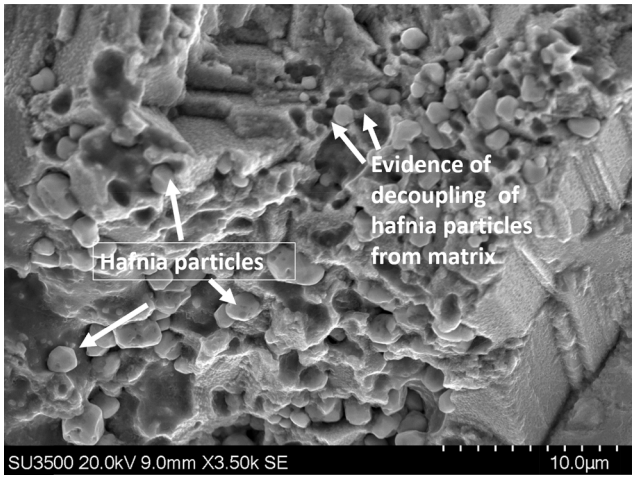

Fig. 7. Initiation of subsurface fatigue cracking from hafnia based inclusion where matrix/inclusion decoupling has occurred.

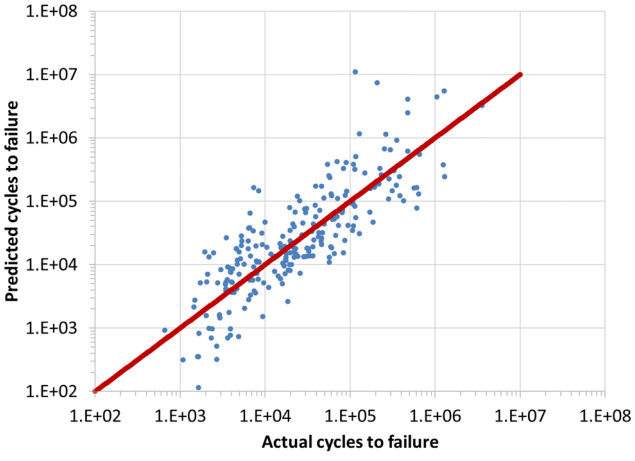

Fig. 8. Prediction of fatigue lives in FG RR1000 at 600–750 °C utilising a single, temperature dependent version of the Walker strain equation.

constitutive equations which can be used for lifing approaches. However, in service components inherently encompass a range of geometrical features which lead to localised increases in stress, and it is therefore critical that such a lifing approach is capable of providing adequate predictions for these features, represented here by notched specimen geometries. A previously published simplistic approach to lifing notched specimen behaviour [15] has utilised Neuber's assumption [27] that at the notch root the product of stress and strain is a constant, therefore allowing for an approximation of the evolution of stress strain conditions under fatigue loading and the appropriate input stresses for the Walker strain equation to allow for the prediction of notched fatigue lives. A more detailed description of the methodology is available in previous work [28].

With the clear demarcation between surface failures and subsurface melt anomalies, it is interesting to consider the validity of notched specimen prediction, particularly at longer fatigue lives where the melt anomaly failures dominated in the plain specimens. Since in the plain specimen the stress field is essentially homogeneous there is an equal opportunity for any melt anomaly to initiate the dominant fatigue crack which leads to failure. However, in the notched specimens considered here ($Kt = 2.29$ and 3.36), plotted as Walker strain vs cycles to failure in Fig. 9, the rapidly decaying stress field away from the notch root means that it is statistically less likely that the critically stressed volume of material will contain a melt anomaly, and therefore an increase in fatigue life, particularly in the HCF region of the fatigue curve is likely.

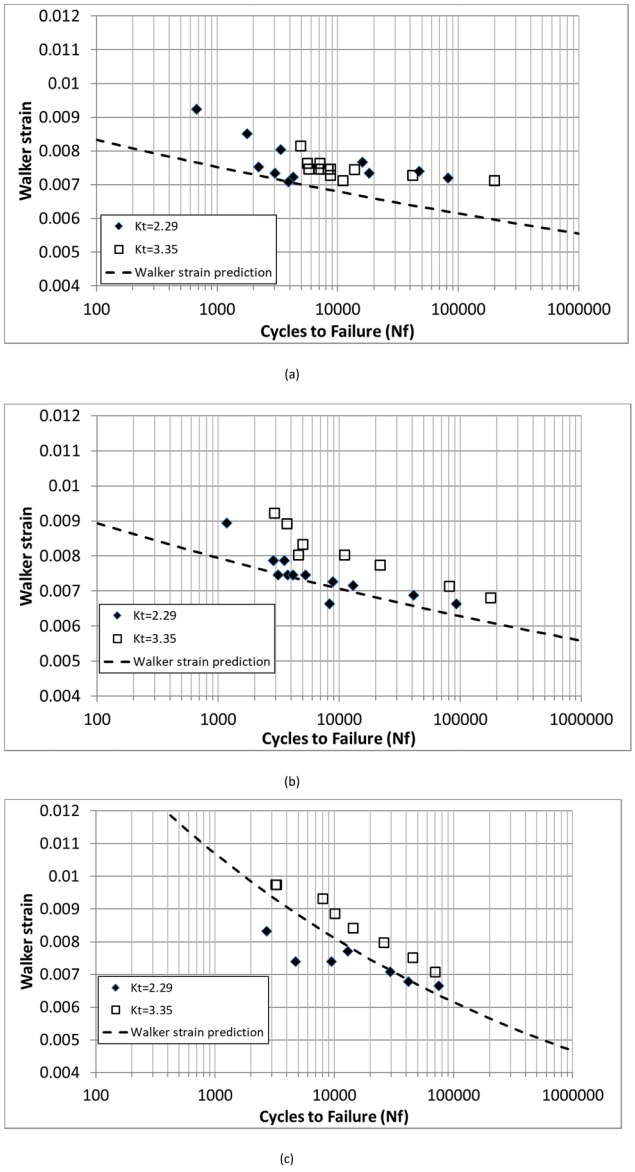

Fig. 9. Walker strain predictions using Neuber approximation for notched specimen ($Kt = 2.29$ and 3.35) fatigue lives at (a) 650 °C (b) 700 °C and (c) 750 °C.

Predictions are included for R = 0 data at three separate temperatures, 650 °C, 700 °C and 750 °C. Due to the fact that strain control data shows only a very limited propagation life, predictions of notched specimen behaviour should only be considered as predictions of crack initiation. Adding a propagation phase to the predictions is a possibility, however, this will vary as a function of applied stress, and is therefore difficult and unreliable. It is however extremely likely that the increase in fatigue lives shown by the notched specimens at the shortest lives is due to early crack initiation and an extended crack propagation phase which is not considered by the predictions. Qualitative predictions however can be made, with the aim of providing conservative estimates.

At 650 °C it is clear that the plain specimen data does indeed underpredict notched specimen HCF lives, however this underprediction is also apparent for LCF lives. Interestingly at this temperature, both $Kt = 2.29$ and 3.35 specimens show similar fatigue lives, whereas when the temperature is increased to first 700 °C and then 750 °C, the fatigue life of the $Kt = 3.35$ specimens is superior to the $Kt = 2.29$ specimens. This is most likely due to the increase in creep deformation at high temperature, where the effect causes a reduction in stress at the notch root through creep softening, with the sharper notch producing a more significant effect. This effect is exacerbated at high stresses where creep rates will significantly increase, and further contributes to the perceived extension in fatigue life due to the extended propagation phase, when compared to the plain specimen predictions under LCF conditions.

At 750 °C the predictions made by the plain specimen data are reasonably accurate, if slightly non-conservative for the high stress $Kt = 2.29$ specimens, where high nominal stresses in the bulk specimen combined with the high creep rates experienced in the alloy at this temperature leads to overall increases in damage in the specimen and a reduced fatigue life. More interestingly, the more accurate predictions seen, when compared to the 650 °C and 700 °C data may be facilitated by the fact that plain specimens showed few failures from melt anomalies at this temperature, thus providing a more direct comparison for the notched specimen failures.

5. Conclusions

The following conclusions can be drawn from the work:-

- A clear distinction occurs for failure locations in FG RR1000. For LCF conditions, failures are dominated by crack initiation from the peened surface. For HCF failures cracks usually initiate from melt anomalies, which have been classified as non-metallic inclusions. The only exceptions are at 750 °C where surface crack initiation was seen at longer lives, and where melt anomalies are located at the surface of the specimen, causing premature failure.
- The Walker strain equation is an appropriate method for lifing the material over a range of temperatures, and a temperature dependent version of the Walker strain equation has been derived which produces good predictive capability over the temperature range 600–750 °C. The continuity of the Walker strain equation was not affect however by the transition from surface to subsurface failures. Lower temperature behaviour (400 °C) does not correlate so well because of general change of behaviour in the alloy to cyclic hardening, and should be considered individually.
- Conservative predictions of notched specimen behaviour have been made using the Walker strain approach, utilising the Neuber assumption for conditions at the notch root. Predictions are affected by the relative contributions of crack initiation and propagation in

the notched specimens, and by the onset of bulk creep in the specimen.

Declaration of Competing Interest

The authors declare the following financial interests/personal relationships which may be considered as potential competing interests: Emily Duffy reports financial support was provided by Rolls Royce plc.

Data availability

The data that has been used is confidential.

Acknowledgements

This work was supported by the UK Technology Strategy Board (SILOET II Project 6 - High Temperature Capability – Compressors and Discs, TP110120). A PhD stipend for Emily Duffy under the EPSRC Rolls-Royce Strategic Partnership in Structural Metallic Systems for Gas Turbines (grants EP/H500383/1 and EP/H022309/1) is also gratefully acknowledged along with funding from Rolls-Royce plc. The input of Dr Mark Evans is also gratefully acknowledged.

References

[1] European Commission/Group of personalities, European aeronautics: A vision for 2020, ACARE; 2004.
[2] European Union, Flightpath 2050 Europe's Vision for Aviation, Report of the High Level Group on Aviation Research; 2011.
[3] Hardy M, Zirbel B, Shen G, Shankar R. Developing damage tolerance and creep resistance in a high strength nickel alloy for disc applications. In: Green KA, Pollock TM, Harada H, Howson TE, Reed RC, Schirra JJ, Walston S. Superalloys 2004, USA; 2004, p. 83–90.
[4] Kuo Y, Kakehi K. Influence of Powder Surface Contamination in the Ni-Based Superalloy Alloy718 Fabricated by Selective Laser Melting and Hot Isostatic Pressing. Metals 2017;7(9):367–79.
[5] Gabb TP, Telesman J, Kantzos PT, Bonacuse PJ, Barrie RL. Initial Assessment of the Effects of Nonmetallic Inclusions on Fatigue Life of Powder-Metallurgy-Processed Udimet(TM) 2002;720.
[6] Lautridou JC, Guedou JY, Honnorat Y. Effect of inclusions on LCF life of PM superalloy for turboengine discs. In: Bachelet E. et al (Eds.), High Temperature Materials for Power Engineering; 1990. p. 163.
[7] Jablonski DA. The Effect of Ceramic Inclusions on the Low Cycle Fatigue Life of Low Carbon Astroloy Subjected to Hot Isostatic Pressing. Mater Sci Eng 1981;48:189–98.
[8] Hyzak JM, Bernstein IM. The effect of defects on the fatigue crack initiation process in two p/m superalloys: part ii. surface-subsurface transition. Metall Mater Trans A 1982;13:45–52.
[9] Jha SK, Caton MJ, Larsen JM. A new paradigm of fatigue variability behavior and implications for life prediction. Mater Sci Eng: A 2007;468–470:23–32.
[10] Shamblen CE, Chang DR. Effect of inclusions on LCF life of HIP plus heat treated powder metal rené 95. Metall Mater Trans B 1985;16:775–84.
[11] Huron ES, Roth PG. The Influence of Inclusions on Low Cycle Fatigue Life in a P/M Nickel-Base Disk Superalloy. In: Kissinger RD, Deye DJ, Anton DL, Cetel AD, Nathal MV, Pollock TM, Woodford DA. Superalloys 1996, The Minerals, Metals and Materials Society; Warrendale, Pennsylvania, USA; 1996. p. 359–68.
[12] BS7270:1990. British standard method for constant amplitude strain controlled fatigue testing. British Standards Institution.
[13] Morrissey RJ, Golden PJ. Effects of Temperature and Frequency on the HCF Behavior of a Ni-based Superalloy. In Evaluation, Control and Prevention of High Cycle Fatigue in Gas Turbine Engines for Land, Sea and Air Vehicles. Meeting Proceedings RTO-MP-AVT-121, Paper 32. Neuilly-sur-Seine; 2005. p. 32-1–32-10.
[14] Walker K. Effects of environment and complex load history on fatigue life. ASTM STP 1970;462:1–14.
[15] Whittaker M. Considerations in fatigue lifing of stress concentrations in textured titanium 6–4. Int J Fatigue 2011;33(10):1384–91.
[16] Lancaster RJ, Whittaker MT, Perkins KM, Jeffs SP. Prediction of fatigue lives at stress raising features in a high strength steel. Int. J. Fatigue 2014;59:301–8.
[17] Basquin O.H. The exponential law of endurance test. In: Proceedings of American society for testing and materials, Philadelphia, vol. 10, 1919, pp. 625–630.
[18] Manson SS. Fatigue: a complex subject – some simple approximations. Exp Mech 1965;5:193–226.
[19] Coffin LF. Fatigue at high temperatures. Fatigue Elevated Temp ASTM STP; 1973. p. 520:5–34.
[20] Morrow J. Fatigue properties of metals, Section 3.2. In: Fatigue design handbook, Pub. No. AE-4, SAE, Warrendale, PA; 1968.
[21] Hurley PJ, Whittaker MT, Williams SJ, Evans WJ. Prediction of fatigue initiation lives in notched Ti 6246 specimens. Int J Fatigue 2008;30(4):623–34.
[22] Qiu C. Net-shape hot isostatic pressing of a nickel based powder superalloy. PhD thesis, University of Birmingham; 2010.
[23] Zhang T, Collins DM, Dunne FPE, Shollock BA. Crystal plasticity and high-resolution electron backscatter diffraction analysis of full-field polycrystal Ni superalloy strains and rotations under thermal loading. Acta Mater 2014;80:25–38.
[24] EASA Certification Memorandum No: CM-PIFS-013 Issue 01 Issued 27 October 2017.
[25] Jones JP, Whittaker MT, Lancaster RJ, Williams SJ. The influence of phase angle, strain range and peak cycle temperature on the TMF crack initiation behaviour and damage mechanisms of the nickel-based superalloy, RR1000. Int J Fatigue 2017;98:279–85.
[26] Zhang T, Jiang J, Britton B, Shollock B. Dunne F Crack nucleation using combined crystal plasticity modelling, high-resolution digital image correlation and high-resolution electron backscatter diffraction in a superalloy containing non-metallic inclusions under fatigue. Proc R Soc A 2015;472:0792.
[27] Neuber H. Trans, ASME, J Appl Mech 1968:544–50.
[28] Whittaker MT, Evans WJ, Hurley PJ, Flynn D. Prediction of notched specimen behaviour at ambient and high temperatures in Ti6246. Int J Fatigue 2007;29(9–11):1716–25.